Chapter 17
Magnetic Semiconductors

Abstract Materials and properties of two types of semiconductors with spontaneous magnetization or ferromagnetic and paramagnetic properties are explained: Compound materials and diluted magnetic semiconductors. A short introduction to semiconductor spintronics covers the concepts of spin transistor and spin LED.

17.1 Introduction

Magnetic semiconductors exhibit spontaneous magnetic order. Even ferromagnetism, important for spin polarization, as needed in spinelectronics (also called *spintronics*), can occur below the Curie temperature that is characteristic of the material. Magnetic semiconductors can be binary compounds such as EuTe (antiferromagnetic) or EuS (ferromagnetic). Another class of magnetic semiconductors contains paramagnetic ions in doping concentration (typically $< 10^{21}\,\mathrm{cm}^{-1}$) or alloy concentration x (typically $x \geq 0.1\%$). Such materials are termed *diluted magnetic semiconductors* (DMS). The incorporation of the magnetic atoms leads first to conventional alloy effects, such as the modification of the lattice constant, the carrier concentration or the band gap. The status of the field up to the mid-1980s can be found in [1516, 1517], mostly focused on II–VI DMS. A review of work on III–V based materials for spintronics, mostly GaAs:Mn, can be found in [1518]. A 2003 review of wide band gap ferromagnetic semiconductors is given in [1519], a 2014 review of Mn-containing DMS in [1520].

17.2 Magnetic Semiconductors

In a magnetic semiconductor, one sublattice is populated with paramagnetic ions. The first two ferromagnetic semiconductors discovered were $CrBr_3$ [1521] in 1960 and EuO [1522] one year later. Europium monoxide has an ionic $Eu^{2+}O^{2-}$ character, such that the electronic configuration of europium is $[Xe]4f^7 5d^0 6s^0$ and that of oxygen is $1s^2 2s^2 2p^6$. Some properties of europium chalcogenides [1523] are summarized in Table 17.1.

EuO can be modeled as a Heisenberg ferromagnet with dominant nearest- and next-nearest Eu–Eu interactions [1524]. The Heisenberg exchange parameters J_1 and J_2 for these four compounds are shown in Fig. 17.1. In the nearest-neighbor interaction J_1 a 4f electron is excited to the 5d band, experiences an exchange interaction with the 4f spin on a nearest neighbor and returns to the initial state. This mechanism generally leads to ferromagnetic exchange. The next-nearest-neighbor interaction J_2 is weakly ferromagnetic (EuO) or antiferromagnetic (EuS, EuSe, EuTe). In the superexchange process,

© Springer Nature Switzerland AG 2021

M. Grundmann, *The Physics of Semiconductors*, Graduate Texts in Physics,
https://doi.org/10.1007/978-3-030-51569-0_17

Table 17.1 Material properties of Eu chalcogenides. 'FM' ('AF') denotes ferromagnetic (antiferromagnetic) order. T_C (T_N) denotes the Curie (Néel) temperature. Data collected in [1525]

Material	E_g (eV)	Magnetic order	T_C, T_N (K)
EuO	1.12	FM	69.3
EuS	1.65	FM	16.6
EuSe	1.8	AF	4.6
		FM	2.8
EuTe	2.00	AF	9.6

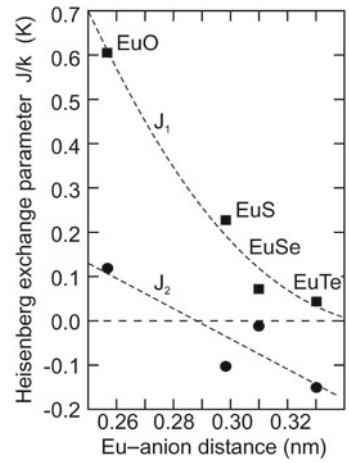

Fig. 17.1 Heisenberg nearest (J_1, *squares*) and next-nearest (J_2, *circles*) exchange parameters (in units of $J_{1,2}/k_B$) for the Eu chalcogenides versus the Eu–anion distance. *Dashed lines* are guides to the eye. Experimental data from [1525]

Table 17.2 3d, 4d and 5d transition metals and their electron configurations. Note that Hf^{72} has an incompletely filled 4f-shell with $4f^{14}$

Sc^{21}	Ti^{22}	V^{23}	Cr^{24}	Mn^{25}	Fe^{26}	Co^{27}	Ni^{28}	Cu^{29}	Zn^{30}
3d	$3d^2$	$3d^3$	$3d^4$	$3d^5$	$3d^6$	$3d^7$	$3d^8$	$3d^9$	$3d^{10}$
$4s^2$	$4s^2$	$4s^2$	4s	$4s^2$	$4s^2$	$4s^2$	$4s^2$	4s	$4s^2$
Y^{39}	Zr^{40}	Nb^{41}	Mo^{42}	Tc^{43}	Ru^{44}	Rh^{45}	Pd^{46}	Ag^{47}	Cd^{48}
4d	$4d^2$	$4d^3$	$4d^4$	$4d^5$	$4d^6$	$4d^7$	$4d^8$	$4d^9$	$4d^{10}$
$5s^2$	$5s^2$	5s	5s	5s	5s	5s	–	5s	$5s^2$
La^{57}	Hf^{72}	Ta^{73}	W^{74}	Re^{75}	Os^{76}	Ir^{77}	Pt^{78}	Au^{79}	Hg^{80}
5d	$5d^2$	$5d^3$	$5d^4$	$5d^5$	$5d^6$	$5d^7$	$5d^8$	$5d^9$	$5d^{10}$
$6s^2$	$6s^2$	$6s^2$	$6s^2$	$6s^2$	$6s^2$	$6s^2$	6s	6s	$6s^2$

electrons are transferred from the anionic p states to the 5d states of the Eu^{2+} cations, resulting in an antiferromagnetic coupling.

17.3 Diluted Magnetic Semiconductors

In Table 17.2, the transition metals and their electron configurations are summarized. The 3d transition metals are typically used for magnetic impurities in DMS due to their partially filled 3d shell. Due to Hund's rule, the spins on the 3d shell are filled in parallel for the first five electrons up to half filling (in

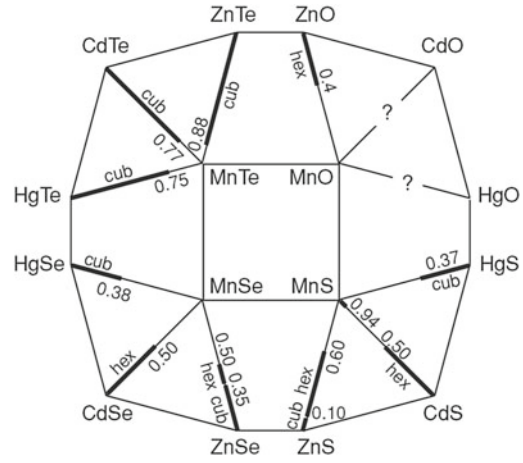

Fig. 17.2 Diagrammatic overview of $A^{II}_{1-x}Mn_xB^{VI}$ alloys and their crystal structures. The *bold lines* indicate ranges of the molar fraction x for which homogeneous crystal phases form. 'Hex' and 'Cub' indicate wurtzite and zincblende, respectively. From [1526]

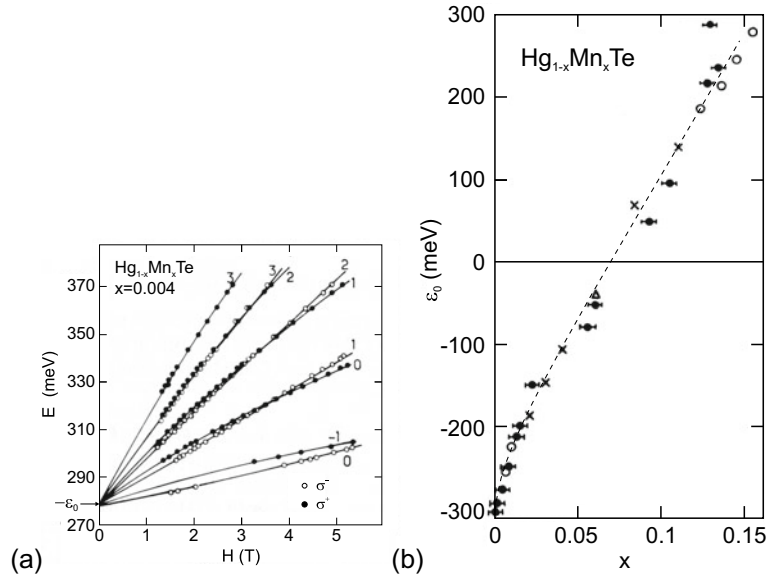

Fig. 17.3 **a** Energies of $\Gamma_6 \rightarrow \Gamma_8$ transitions versus magnetic field for $Hg_{0.996}Mn_{0.004}Te$ at $T = 2\,K$. *Symbols* are experimental values for two polarization directions as indicated. Numbers denote quantum numbers of transitions. *Solid lines* are theoretical fits. **b** Interaction gap versus Mn concentration for $Hg_{1-x}Mn_xTe$ at $T = 4.2\,K$. Various *symbols* represent data from different authors and methods. *Dashed line* is a guide to the eye. Adapted from [1528]

order to allow the electrons to get out of their way in real space). Thus, the atoms have a sizeable spin and a magnetic moment. The spin of Mn is $S = 5/2$. Most transition metals have a $4s^2$ configuration that makes them isovalent in II–VI compounds. We note that Zn has a complete 3d shell and thus no net spin. In Fig. 17.2, an overview of the crystallographic properties is given for Mn-alloyed II–(Se, S, Te, O) based DMS [1526] (DMS with Se, S, and Te have been discussed in [1527]).

As an example, the properties of $Hg_{1-x}Mn_xTe$ are discussed. This alloy is semiconducting (positive band gap ϵ_0) for $x > 0.075$ and a zero-gap material (negative interaction gap ϵ_0) for smaller Mn concentration (cf. Fig. 6.46). The transitions between the Γ_6 and Γ_8 bands can be determined with magnetoabsorption spectra in the infrared [1528]. In Fig. 17.3a, the magnetic field dependence of transition energies between different Landau levels is shown that can be extrapolated to yield the interaction gap. The interaction gap is shown in Fig. 17.3b as a function of the Mn concentration.

For small Mn concentrations, the DMS behaves like a paramagnetic material. For larger concentrations, the Mn atoms have increasing probability to be directly neighbored by another Mn atom and suffer superexchange interaction (cf. (3.24b)). At a certain critical concentration x_c, the cluster size

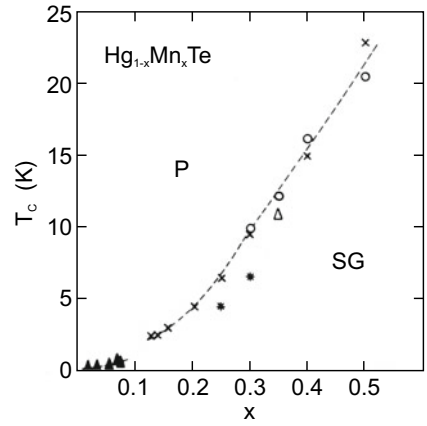

Fig. 17.4 Magnetic phase diagram of $Hg_{1-x}Mn_xTe$, 'P' ('SG') denotes the paramagnetic (spin glass) phase. Various *symbols* represent data from different authors and methods. *Dashed line* is a guide to the eye. Adapted from [1528]

becomes comparable with the size of the sample. If interaction up to the first, second or third neighbor are taken into account for a fcc lattice, the critical concentrations are given by $x_c = 0.195$, 0.136, and 0.061, respectively [1529]. The nearest-neighbor interaction between Mn atoms in such DMS as (Zn, Cd, Hg) Mn(S, Se, Te) was found to be antiferromagnetic,[1] i.e. neighboring spins are aligned antiparallel. Due to frustration of antiferromagnetic long-range order on a fcc lattice, an antiferromagnetic spin glass forms. The transition temperature T_C between the paramagnetic and spin-glass phases of $Hg_{1-x}Mn_xTe$ is shown in Fig. 17.4.

In III–V compounds, the 3d transition metals represent an acceptor if incorporated on the site of the group-III element as, e.g., in the much investigated compound $Ga_{1-x}Mn_xAs$. This material will be used in the following to discuss some properties of magnetic semiconductors. It seems currently well understood and has a fairly high Curie temperature of $T_C \approx 160\,K$. Ferromagnetism in a diluted magnetic semiconductor is believed to be caused by indirect exchange through itinerant charge carriers. The ferromagnetic coupling can be invoked by the Ruderman–Kittel–Kasuya–Yoshida (RKKY) interaction, i.e. the spins of the paramagnetic ions are aligned via interaction with the free carriers in the semiconductor. A related concept is the double exchange[2] [1530–1532] in which carriers move in a narrow Mn-derived d-band (for d-wave character see Fig. 7.16c). Such a mechanism was first invoked for PbSnMnTe [1533]. Later, ferromagnetism was discovered in InMnAs [1534] and GaMnAs [1535]. In (In,Ga)MnAs a Mn ion (spin up) spin polarizes the surrounding hole gas (spin down), which has been supplied from the Mn acceptors. This mechanism lowers the energy of the coupled system. The interaction

$$H = -\beta\, N_0\, x\, S\, s \tag{17.1}$$

between the Mn d-shell electrons ($S = 5/2$) and the p-like free holes ($s = 1/2$) is facilitated by p–d hybridization of the Mn states. N_0 denotes the concentration of cation sites in the $A_{1-x}Mn_xB$ alloys. The coupling via electrons is much weaker (coupling coefficient α). The holes interact with the next Mn ion and polarize it (spin up), thus leading to ferromagnetic order. The ferromagnetic properties are evident from the hysteresis shown in Fig. 17.6a. Without the carrier gas such interaction is not present and the material is only paramagnetic. Theoretical results for the Curie temperature of various p-type semiconductors are shown in Fig. 17.5. Generally, the quest for higher Curie temperatures (well above room temperature) is underway and wide band gap materials such as GaN or ZnO doped with transition metals have shown some encouraging results. Mn-substituted chalcopyrite semiconductors

[1] Such superexchange leads to antiferromagnetic interaction if the bond angle is 'close' to 180°.

[2] This model is also called the Zener model.

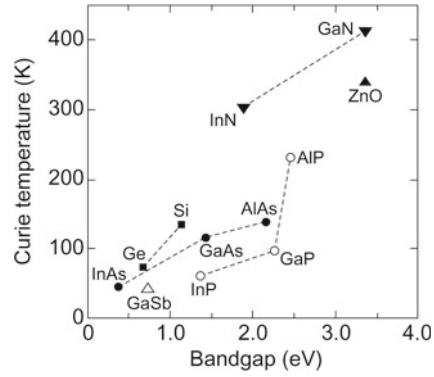

Fig. 17.5 Computed values of the Curie temperature T_C for various p-type semiconductors plotted versus the band gap (*dashed lines* are guides to the eye). All materials contain 5% Mn on the cation sublattice and a hole concentration of $p = 3.5 \times 10^{20}\,\mathrm{cm}^{-3}$. Values for T_C taken from [1532]

are analyzed theoretically in [1536] and are predicted to exhibit less-stable ferromagnetism than III–V semiconductors of comparable band gap.

The carrier density and thus magnetic properties in a DMS can be controlled in a space-charge region (cf. Sect. 21.2.2) as demonstrated in [1537]. In Fig. 17.6, results are shown for hydrogen- (deuterium-) passivated GaMnAs that exhibits ferromagnetism as 'as-grown' thin film. The deuterium is incorporated in similar concentration as the Mn, assumes a back-bond position (forming a H–As–Mn complex) and compensates the hole gas from the Mn (cf. Sect. 7.9). The low-temperature conductivity drops nine orders of magnitude [1538]. Such material displays only paramagnetic behavior. An optimal Mn concentration for ferromagnetic $Ga_{1-x}Mn_xAs$ is around $x = 0.05$. For smaller Mn concentrations, the hole density is too small and the Curie temperature drops; for larger Mn concentrations, the structural properties of the alloy degrade (phase separation into GaAs and MnAs.[3]).

Magnetic hysteresis has been found in nearly compensated Mn-doped ZnO [1539, 1540] (Fig. 17.7). Such material is interesting due to its small spin-orbit coupling. The exchange mechanism is under debate.

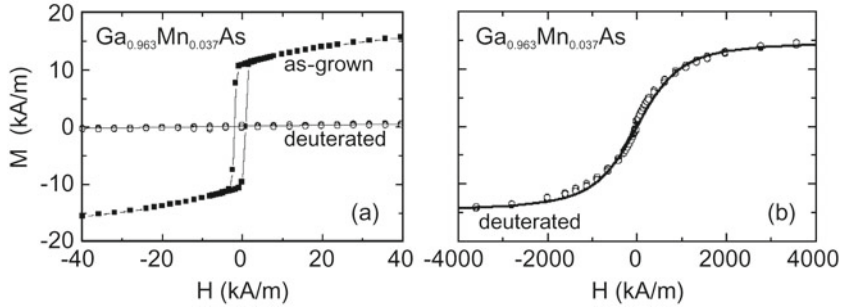

Fig. 17.6 Magnetization M versus magnetic field H for $Ga_{0.963}Mn_{0.037}As$ at low temperature. **a** Comparison of as-grown (*full squares*) and deuterated (*open circles*) thin film with magnetic field in the layer plane at $T = 20\,\mathrm{K}$. **b** Magnetization of the deuterated sample at $T = 2\,\mathrm{K}$ for larger magnetic fields. *Solid line* is Brillouin function for $g = 2$ and $S = 5/2$. Adapted from [1538]

[3] MnAs is a ferromagnetic metal. MnAs clusters can be a problem since they create ferromagnetic properties but not in the way the DMS is supposed to work.

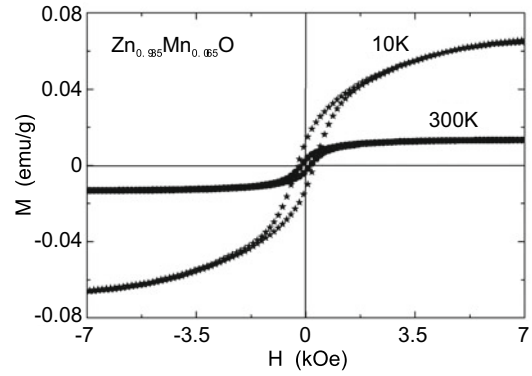

Fig. 17.7 Magnetization M versus magnetic field H for $Zn_{0.935}Mn_{0.065}O$ thin film at $T = 10$ and 300 K. A hysteresis is obvious for both temperatures

17.4 Spintronics

Spintronics (as opposed to electronics) is an emerging field that uses the electron *spin* rather than its *charge* for transport, processing and storage of information. Prototype devices are the spin transistor and the spin LED. A crucial point is spin injection, i.e. the creation of (highly) spin-polarized currents. It remains to be seen whether spintronics can be developed to its theoretically envisioned potential and will play a commercially important role in the course of microelectronics. The spin degree of freedom also promises potential for quantum information processing due to its weak coupling to charge and phonons and the resulting long dephasing time.

It shall be mentioned here that the magnetization alters also the 'classical' transport properties of the semiconductor. The Hall effect is modified strongly and reflects the magnetic hysteresis, also termed *anomalous* Hall effect (AHE).[4] This effect was already discovered by Hall in 1881 for Ni and Co [1541]; a review of the AHE can be found in [1542]. Also the optical excitation of spin-polarized carriers in non-magnetic materials causes AHE [1543]. For a magnetic material with topological band structure, the internal field can be sufficient to evoke the QHE [1544]; this quantum anomalous Hall effect (QAHE) has been reported for $(Bi,Sb)_2Te_3$:Cr [1545] and $MnBi_2Te_4$ [1546].

17.4.1 Spin Transistor

In this device (for regular transistors cf. Chap. 24), spin-polarized electrons are injected from contact 1, transported through a channel and detected in contact 2. During the transport, the spin rotates (optimally by π) such that the electrons cannot enter contact 2 that has the same magnetization as contact 1 (Fig. 17.8). The spin rotation is caused by spin-orbit interaction due to the electric field under the gate contact. This effect is called the Rashba effect and is purely relativistic [1547]. As channel material, a semiconductor with strong spin-orbit coupling such as InAs or (In,Ga)Sb is preferable. However, the use of narrow-gap semiconductors and the increase of spin scattering at elevated temperatures [1548] make the realization of such a transistor at room temperature difficult.

[4] This use of the term 'anomalous' should be distinguished from the historical use of 'anomalous' Hall effect for the sign reversal of the Hall voltage for hole conductors.

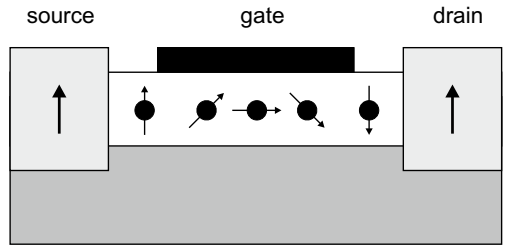

Fig. 17.8 Scheme of spin transistor after the proposal of [1549]. Source and drain are ferromagnets with their magnetization shown schematically as arrows. The channel under the gate transports electrons whose spin rotates in the electric field under the gate

17.4.2 Spin LED

In a spin LED (for LEDs see Sect. 23.3), the injection of spin-polarized carriers into the active layer leads to circularly polarized luminescence. The spin alignment can be achieved with semimagnetic semiconductors grown on top of the active layer or via spin injection from a ferromagnetic metal into the semiconductor (for metal–semiconductor junctions cf. Sect. 21.2). In Fig. 17.9a, a Fe/AlGaAs interface is shown.

Ideally, the spin-polarized electrons from the ferromagnetic metal tunnel into the semiconductor and transfer to the recombination region. Subsequently, the emission is circularly polarized (Fig. 12.30b). The degree of circular polarization is

$$P_\sigma = \frac{I_{\sigma+} - I_{\sigma-}}{I_{\sigma+} + I_{\sigma-}} , \tag{17.2}$$

with $I_{\sigma\pm}$ being the intensity of the respective polarization. The degree of polarization depends on the magnetization of the metal. For the saturation magnetization of Fe, the maximum polarization is about

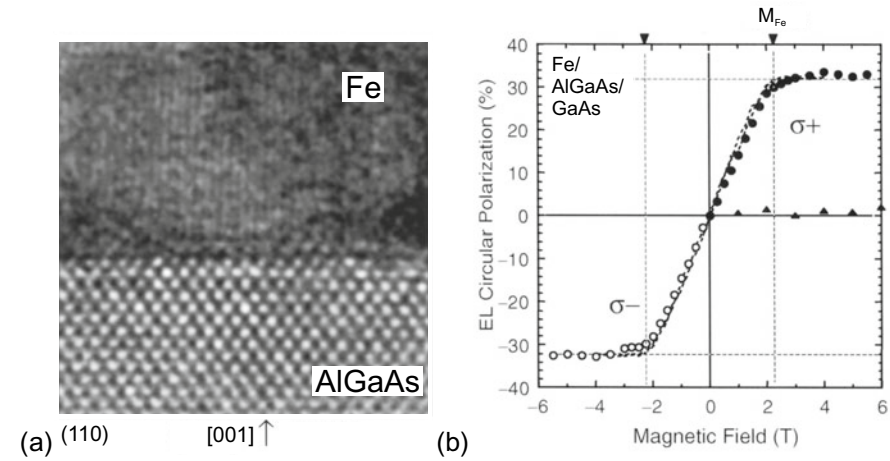

Fig. 17.9 **a** Transmission electron microscopy image of the (110) cross section of the Fe/AlGaAs interface of a spin LED. The *vertical lines* in Fe are the (110) planes with 0.203 nm distance. **b** Magnetic-field dependence of the circular polarization ratio P_σ at $T = 4.5\,\mathrm{K}$ (17.2) (*filled* and *empty* circles) and the out-of-plane component of the Fe-film magnetization (*dashed line*, scaled to the maximum of P_σ). Reproduced from [1551] by permission of the MRS Bulletin

30% at $T = 4.5\,\mathrm{K}$ (Fig. 17.9b) [1550]. The interface and its structural nonideality of the interface presumably prevent the spin injection from being 100% efficient [1551]. Recently, close to pure (95%) circular polarization has been obtained from a (Al,Ga)As/GaAs-based stripe-laser-like (edge emitting) structure with Fe/crystalline AlO_x spin-tunnel barrier [1552].